J Neurophysiol 94: 3406–3416, 2005.
First published July 27, 2005; doi:10.1152/jn.00264.2005.

Signal Propagation Along Unidimensional Neuronal Networks

Ofer Feinerman,[1] Menahem Segal,[2] and Elisha Moses[1]
[1]*Departments of Physics of Complex Systems and of* [2]*Neurobiology, The Weizmann Institute of Science, Rehovot, Israel*

Submitted 11 March 2005; accepted in final form 17 July 2005

Feinerman, Ofer, Menahem Segal, and Elisha Moses. Signal propagation along unidimensional neuronal networks. *J Neurophysiol* 94: 3406–3416, 2005. First published July 27, 2005; doi:10.1152/jn.00264.2005. Dissociated neurons were cultured on lines of various lengths covered with adhesive material to obtain an experimental model system of linear signal transmission. The neuronal connectivity in the linear culture is characterized, and it is demonstrated that local spiking activity is relayed by synaptic transmission along the line of neurons to develop into a large-scale population burst. Formally, this can be treated as a one-dimensional information channel. Directional propagation of both spontaneous and stimulated bursts along the line, imaged with the calcium indicator Fluo-4, revealed the existence of two different propagation velocities. Initially, a small number of neighboring neurons fire, leading to a slow, small and presumably asynchronous wave of activity. The signal then spontaneously develops to encompass much larger and further populations, and is characterized by fast propagation of high-amplitude activity, which is presumed to be synchronous. These results are well described by an existing theoretical framework for propagation based on an integrate-and-fire model.

INTRODUCTION

The advance of activity through a neural network reveals much about its underlying properties. In particular, the velocity in which a signal propagates may differentiate synchronous from asynchronous activity and can identify the limiting factors in transmission, whether they are synaptic or axonal. The dependency of velocities on the strength of the α-amino-3-hydroxy-5-methyl-4-isoxazolepropionic acid (AMPA) synapses has been experimentally demonstrated in bursts that propagate in slices (Golomb and Amitai 1997).

In this report such questions are addressed using a novel experimental system in which dissociated hippocampal neurons are grown along one-dimensional (1-D) patterned lines. These networks (Chang et al. 2001; Segev et al. 2002) provide a bridge that can link the realistic experimental system to numerous theoretical modeling approaches, which often deal effectively with one dimension (Abeles 1991; Diesmann et al. 1999; Golomb and Amitai 1997; Litvak et al. 2003; Osan and Ermentrout 2002; Siegal and Read 2001). Viewed as simplified models of cortical structure, such theoretical networks were used to address questions concerning the possible cortical coding schemes (Abeles 1991; Diesmann et al. 1999; Litvak et al. 2003).

The major advantage of using one-dimensional cultures to study propagation is that a signal has only a limited pathway. Two-dimensional (2-D) networks and slices exhibit similar activity, but may have a large number of possible paths connecting any two given points (Beggs and Plenz 2004; Buonomano 2003). The relative strength of the paths and their interplay are difficult to measure and complex to model, especially because signal propagation in two dimensions is prone to instabilities (Kistler 2000; Wu et al. 1999). The limitation on propagation pathways can be further exploited by local drug application (Feinerman and Moses 2003). Applying drugs on a single point along a narrow line directly affects only a small number of cells yet it may trigger or otherwise affect activity in the network as a whole.

The first goal of the study reported herein is to characterize the culture and to demonstrate that it is indeed layered and directed along one dimension. This is done by applying pharmacological treatments and by analyzing the architecture of the network. We then go on to study network activity. The culture exhibits bursts of population activity that propagate in a causal fashion, each area exciting the next neighboring one. The second goal of this study is to characterize the propagation of these bursts along the line. This can be done with precision as a result of the chainlike excitation of activity. It turns out that this neuronal architecture can support two different velocities: initially a low-amplitude and slowly propagating activity appears, but it is unstable and eventually gives way to a fully developed, high-amplitude, and fast-moving burst of activity.

Finally, the unidimensional structure allows a quantitative comparison to existing 1-D wave propagation theoretical models, and excellent quantitative agreement was achieved for a model with a fully analytical solution that predicts the coexistence of slow and fast velocities (Osan and Ermentrout 2002). Based on this theory, one can discuss the two velocities in terms of the arrival times of excitatory postsynaptic potentials (EPSPs) to a single neuron, to try to relate the slow and fast velocities with asynchronous and synchronous ("synfire mode"; see Abeles 1991) propagation, respectively. Such a transition in propagation mode was predicted theoretically for a feedforward (1-D) chain (Diesmann et al. 1999).

METHODS

Culture of hippocampal neurons

Primary cultures were prepared following Papa et al. (1995). Briefly, 19-day-old embryos were taken from Wistar rats. The brains were removed, and the hippocampi dissected out and dissociated by mechanical trituration. The dissociated cells were plated onto previously patterned, 13-mm glass coverslips (#1, Menzel-Glaser) at 330,000 cells/ml. The cells were incubated at 37°C, 5% CO_2 in plating medium [Eagle's MEM supplemented by 5% heat-inactivated horse serum, 5% heat-inactivated fetal calf serum, 0.6% glucose, gentamicin (20 μg/ml), glutamax (Gibco), and B27 supplement (1 μl/ml)]. After

Address for reprint requests and other correspondence: O. Feinerman, Department of Physics of Complex Systems, The Weizmann Institute of Science, Rehovot, Israel 76100 (E-mail: feiner@wisemail.weizmann.ac.il).

The costs of publication of this article were defrayed in part by the payment of page charges. The article must therefore be hereby marked "*advertisement*" in accordance with 18 U.S.C. Section 1734 solely to indicate this fact.

3 days the medium was switched to one that contains, apart from 10% heat-inactivated horse serum, FUDR (5-fluoro-deoxy-uridine) and uridine to inhibit further division of glial cells, which are also confined to the micropatterns and serve as a support layer for the neurons. The final change of medium 3 days later included 10% heat-inactivated horse serum, glucose, gentamicin, and glutamax.

Coverslip patterning

As described by Feinerman and Moses (2003), glass coverslips were patterned to make only specific locations (usually lines) available for cell adhesion. This is done in two steps: first the entire coverslip is coated by multiple layers, the topmost being a monolayer of Pluronics F108 Prill (BASF), which makes it inert to proteins and thus unavailable for cell adhesion. Then, using an HP 7475A plotter (Hewlett–Packard), in which the pen was replaced by a sharp metal tip, lines are scratched through this coating in the preprogrammed pattern. The entire coverslip is then immersed in a solution of pluronics laminin and fibronectin, the adhesion proteins attach only to the lines.

The dissociated cells are plated onto these treated coverslips, adhering to the exposed lines only, and within a few days connect along these lines to make linear neural networks. The minimal line width that can support the cell soma for a prolonged period of time is about 50 μm, whereas axons can cross lines that are thinner (see Fig. 1*G*). Lines were patterned with thicknesses ranging between 10 and 300 μm. The repulsion of the Pluronics coating does not fade in time and, despite the possible secretion of adhesion proteins by the cells themselves (Alitalo et al. 1982), the cells remain almost exclusively on the lines throughout their life.

Imaging neuronal activity with calcium-sensitive fluorescent dyes

Two- to 3-wk-old cells were incubated for 60 min in the recording solution (128 mM NaCl, 4 mM KCl, 1 mM $CaCl_2$, 1 mM $MgCl_2$, 45 mM sucrose, 10 mM glucose, and 0.01 M HEPES; pH is titrated to 7.4) in the presence of 2 μg/ml cell-permeant Fluo4-AM [Molecular Probes (now Invitrogen, Carlsbad, CA)], a calcium-sensitive dye. Cells were then washed and placed again in recording solution. The culture was maintained at 28°C and imaged on a Zeiss Axiovert 135TV microscope, photographed through a 10 × lens by a Hamamatsu C2400-87 CCD camera fitted with a 0.5 × adapter to enlarge the field of view. The images were captured at 25 Hz, stored on videotape, and digitized with a PCI-1141 frame grabber (National Instruments) and IMAQ software (Labview). De-interlacing was pre-

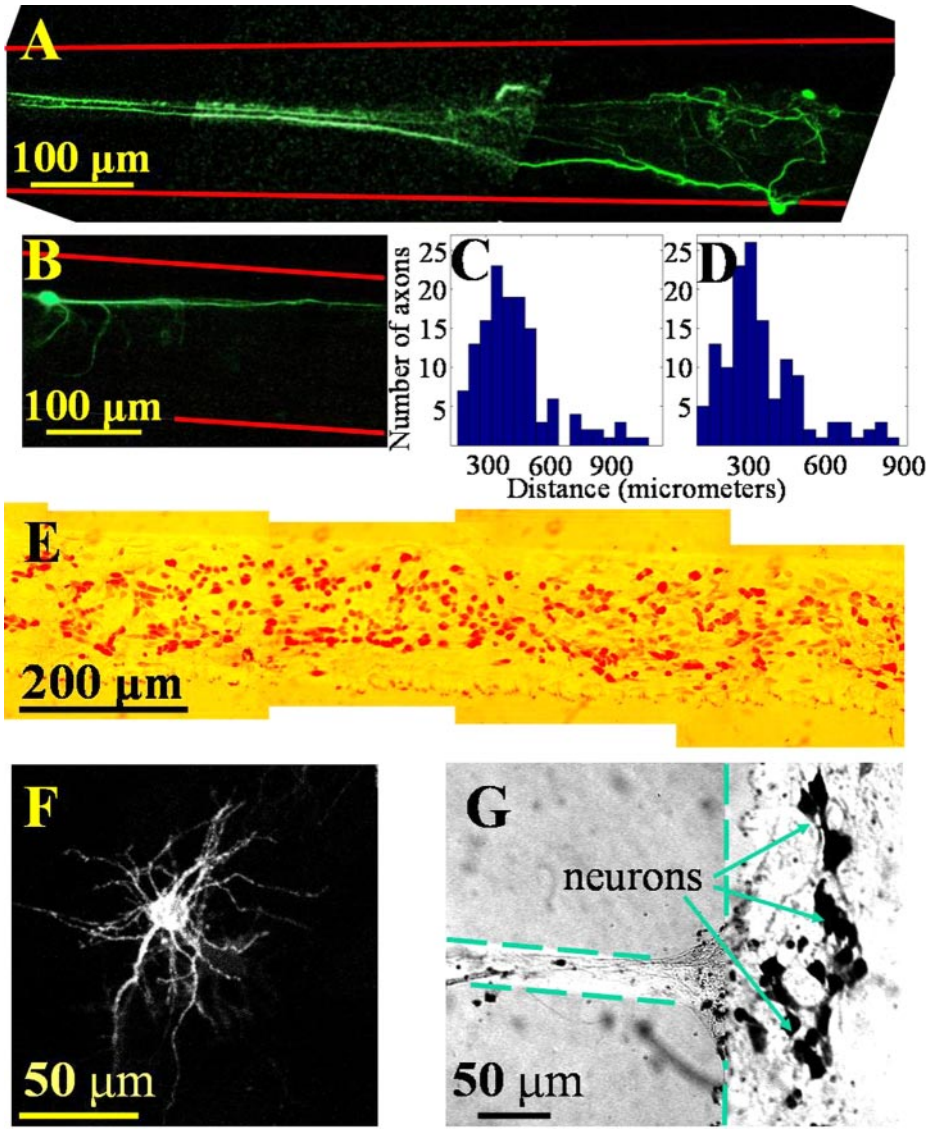

FIG. 1. Structural characterization of neural network on 170-μm-thick lines 9–15 days after plating. Confocal (*A*) and regular (*B*) fluorescence microscope images of Tau-GFP transfected cells 9 days after plating. About 1% of the cells were transfected, allowing a measurement of their axon length. Borders of the line are marked by digital postprocessing (red) as a guide to the eye. The lower axon visualized on *A* has a full length of 780 μm and a projected length of 725 μm, which is 93% of its full length. *B*: digitally postprocessed to eliminate background interference from neighboring neurons. *C*: histogram of the full axon lengths; the mean length is 360 μm. *D*: histogram of the projected length of axonal processes along the line. Axons usually grow parallel to the line so that their mean projected length, 308 μm, is close to their mean length. *E*: all the neurons in the network are stained with Neu-N (neuron-specific nuclear protein) to demonstrate their density/distribution. *F*: a single neuron stained with a microdrop of DiI (1-didodecyl-3,3,3′,3′-tetramethyl indocarbocyanine), photographed 1 h later using a confocal microscope. *G*: lines under 50 μm usually do not support cell adhesion. Shown is a junction between a thick (170 μm) and a thin line (30 μm); both lines are emphasized by digital postprocessing by dashed lines. Neu-N–stained neurons are visible on the thick line (arrows), whereas the thin line supports only axons (and perhaps dendrites).

formed to raise the time resolution to 50 Hz before subsequent off-line analysis.

Pharmacology

Several drugs were applied to ensure that the patterned culture was synaptically active. AMPA, *N*-methyl-D-aspartate (NMDA), and γ-aminobutyric acid (GABA) receptors were blocked by bath application of their respective antagonists: 2 μM of 6-cyano-7-nitroquinoxaline-2,3-dione (CNQX), 1–10 μM of 2-amino-5 phosphonovaleric acid (APV), and 40 μM of bicuculline. Voltage-gated sodium channels were blocked by bath application of tetrodotoxin (TTX, 100 nM), whereas 5–100 μM nifedipine was used to block calcium channels. The effect of inhibitory synapses on the culture was tested by bath application of 100 μM of GABA. All drugs were purchased from Sigma except Fluo-4AM (Molecular Probes).

Localized chemical stimulation

A method for local drug application using a specially designated double-pipette system (Feinerman and Moses 2003) was developed. The double pipette can be used for excitation of signals and has many advantages over electrical excitations (Murphy et al. 1992; Wu et al. 1999). Among these is having a large diversity of drugs that are harmless to the neurons while creating many different effects. Local drug application is more natural than global excitation (and happens in real brain).

The system consists of two concentric pipettes of which the inner one, which has a 10-μm-diameter tip and protrudes about 100 μm from the opening of the larger pipette, is used as a regular application pipette that can be filled by any solution. The outer pipette has a tip diameter of about 100 μm and is constantly kept at a pressure lower than atmospheric, which maintains a steady suction of any surrounding liquid. This allows a very controllable and localized flow of any applied solution with no diffusive leak to the surrounding cells.

For stimulation of the culture, the inner pipette was loaded with either 20 or 200 μM L-glutamic acid buffered in recording medium, with similar results for the two concentrations. The flow was calibrated to reach an area with diameter of about 100 μm. Smaller perfusion areas were less likely to stimulate the network. Application times of between 20 ms and 1 s were used, typically 100 ms at a rate of once every 10 s.

For local obstruction of the signal, the inner pipette was loaded with 1 μM of TTX and the flow calibrated to reach an area with diameter of about 200 μm. The drug was continuously applied for periods ≤10 min long.

Imaging structure

IMMUNOCYTOCHEMISTRY AND NEURON STAINING. Cells to be imaged were fixed in 4% paraformaldehyde 14 days after plating. To target neurons specifically, the culture was incubated overnight at 4°C with mouse anti-neuronal nuclei (NeuN, Chemicon), 10% horse serum, and 0.3% Triton. Staining was done using the Vectastain Elite ABC Kit from Vector Laboratories. The samples were then developed for 60 s with DAB (Sigma), dehydrated, and mounted onto coverslips.

GFP AND TAU-GFP TRANSFECTION. Cells were transfected with either nonspecific GFP or Tau-GFP to visualize their dendritic or axonal processes, respectively. In both cases 1.5 μg of the plasmid (pEF/myc/cyto/GFP from Invitrogen) and 1.5 μl of Lipofectamin2000 (Invitrogen) were diluted in 100 μl of optiMEM1 (Gibco). The solution was added to neurons (7–14 days after plating) in 500 μl of the final growing medium. Imaging was done 2 days later.

DII STAINING. DiI (1-didodecyl-3,3,3′,3′-tetramethyl indocarbocyanine) staining was done as previously described (Papa et al. 1995). The dye was immersed in oil at saturated concentrations. A microdrop of the dye was placed on the cell under the microscope and the dye was allowed to spread to the dendrites of the cell for several hours before confocal imaging of the cell.

Data analysis

Analysis of the fluorescence signals was done off-line. Several regions of interest were chosen on the image and their average fluorescent intensity measured. These measurements were taken at 50-Hz resolution by de-interlacing the video image before spatial averaging. An estimate of the mean fluorescence and standard deviation (SD) was calculated for each region of interest. The baseline f_0 was calculated from the total background intensity during nonfiring periods, and the signal f was normalized by $(f - f_0)/f_0$. For every event the algorithm for extracting the initial point finds the first time that the amplitude exceeds 1.5 SDs above the background. It then tracks backward to find the point at which the fluorescence intensity begins to rise, and monotonically increases thereafter. That is designated as the initial point for the signal. A second time point of interest is that at which there is maximum enhancement of the signal, i.e., where the derivative is maximal.

RESULTS

Synopsis

A functional 1-D culture of rat hippocampus ≤8 centimeters long and typically 170 μm wide was developed. The small dimension of this culture is narrow enough so that the system may be considered one-dimensional. The axon-length distribution was measured, characterizing the connectivity on this line. Calcium imaging indicates that the culture is spontaneously active and generates activity that travels the extent of the line, passed by synaptic transmission from neuron to neuron to reach the furthest neurons. These bursts of activity are evident as signals of enhanced fluorescence propagating along the line, and shall be referred to henceforth as propagating signals or waves. We measured the velocity and origin of these spontaneous signals as was done on cortical slices (Chervin et al. 1988; Golomb and Amitai 1997; Metherate and Cruikshank 1999; Wu et al. 1999) and on 2-D and semi–1-D cortical cultures (Maeda et al. 1995). For both spontaneous and evoked events, slowly propagating activity waves were measured close to the site of signal initiation, which then develop into fast waves propagating beyond the initiation site. The velocity measurements were compared with a theoretical 1-D wave-propagation model (Osan and Ermentrout 2002).

Connectivity and density

To obtain a measure of the connectivity of the network, the extent of axons and dendrites was followed separately. The length of axons for Tau-GFP–transfected cells (Fig. 1, *A* and *B*) was measured along a line of width 170 μm. The mean total length of these axons was 360 ± 18 μm ($n = 135$; all averages are presented as means ± SE), with only 6% of the axons extending >800 μm (Fig. 1*C*).

If the axon wanders around along its path then its total length should be greater than the projected distance along the line (projection of the straight line connecting the soma with the furthest point reached by the axon onto the line of the culture). In fact, the projected distance turned out to be very similar to the actual length, indicating that the axons do not wander as

they do in a 2-D culture, and on average 78% of their length is used to advance along the direction of the cultured line. The averaged projected distance traveled by axons is 308 ± 16 μm (n = 135) with <3% of the axons traveling a projected distance longer than 800 μm (Fig. 1*D*). There was no significant difference in these figures between long (17 mm) or short (4 mm) lines. The fact that the axons are considerably directional contributes to the linearity of the network.

Mean dendrite length was measured by using either DiI imaging (Fig. 1*F*) or nonspecific GFP transfections. In the latter case the axonal process, characterized by its length and constant thin width, was not measured. The maximal extension of dendrites from the cell soma was on average 80 ± 4 μm (n = 144 dendrites on 25 neurons), and the longest dendrites reached 200 μm. The dendritic tree is highly branched, and dendrites also extend upward and downward into the z-dimension. The synaptic input basin in fact reaches a diameter on the order of 200 μm, which is the width of the line. This collapses the small dimension of the line and allows it to be referred to as a one-dimensional system. Because the cells are initially seeded and plated uniformly, the width of the small dimension can be transformed into an effective variable describing the linear density of neurons. We assume that an axon that lies along this linear density of neurons has an unknown but fixed probability of connecting to any neuron near its path. The linear density of neurons along the line is thus a reliable parameter describing the transmission capability of this system.

Finally, to count the average number of neurons per unit length (and obtain the linear density) neuronal nuclei were stained using NeuN (Fig. 1*E*). This marker gave the strongest staining for neurons in the topmost layer, with a decrease in staining for cells further down from the surface. Some areas were also very dense, making it hard to differentiate between different cells. Still many of the neurons were easy to visualize and counting of most of the neurons was possible, so this should be a good estimate for the number of neurons.

Neurons from five samples of 170-μm-thick lines with a total length of 18 mm were counted, giving a linear density of 0.31 ± 0.02 neurons per micrometer. This density gives about 6,200 cells on a typical 2-cm-long strip. On thin parts of the line (50 μm width, total length 2.5 mm) the linear density was 0.06 ± 0.01 neurons per micrometer, less by a factor of 5, which is more than the ratio of widths. Thus neuron density does not scale with the width of the line as it narrows down, and there is usually no adhesion of cells to lines that are thinner than 50 μm; axons, on the other hand are supported by lines as narrow as 10 μm (Fig. 1*G*).

We conclude that the line width gives a good control over the linear neuron density, and in this way a handle on the connectivity and the signal transmission properties of the network.

Taking into account the intricate dendritic network of each cell, an upper limit on the mean number of neurons onto which a single cell can make a synapse can be estimated. This can be done by assuming that it reaches every neuron distanced up to the mean axon plus dendrite length. This gives an upper bound on the average connectivity at $(308 + 80) \times 0.31 \approx 120$ cells that may be connected to an axon on a 170-μm-wide line.

Spontaneous activity and the effect of drugs

The linear networks constructed in this fashion exhibit clear and strong spontaneous activity at a characteristic frequency, interspersed with long quiescent periods. The activity, once it develops into the fast high-amplitude mode (see following text), is typically "all or none", traveling the full extent of the line, with the exception of constrictions discussed in the following text. This is similar to results reported by others (Maeda et al. 1995; Menendez de la Prida and Sanchez-Andres 2000; Murphy et al. 1992). The interevent interval was 18 ± 3 s on average, as measured on ten short lines (length 4 mm) and nine long lines (length 17 mm), with no observable difference between long and short lines.

The effect of several drugs on the behavior of the cultures was tested to verify the normal activity of the neurons and their synapses. For all the treatments described below the effect of the drugs was reversible on washing (data not shown).

Blocking NMDA receptors with 1 μM of APV, as tested on three cultures, caused an average decrease of 30% in the amplitude of the fluorescence signals (Fig. 2*A*). Increasing the concentration to 10 μM caused a further decrease, down to 50% of the original amplitudes, which indicates that the NMDA synapses are involved in the calcium variations in these cells.

Adding 2 μM of the AMPA receptor antagonist CNQX caused a complete halt in spontaneous network activity (tested on six cultures) (data not shown).

Bicuculline (40 μM), which blocks inhibitory GABA synapses, was added to more than 20 cultures, resulting in an increase in signal amplitudes that ranged between 1.5- and fivefold over control measurements (Fig. 2*B*). Addition of 100 μM GABA caused a complete cessation of spontaneous activity (data not shown).

TTX at 2 μM caused a complete halt of network activity, either spontaneous or evoked (n = 10). A lower concentration of 10 nM allowed a local stimulation of an area of the culture using the glutamate-loaded coaxial pipettes, but blocked propagation of all activity to other parts of the culture (Fig. 2*C*).

Finally, 5 μM of nifedipine (NIF), as tested on three cultures, did not induce a very pronounced change, but did decrease amplitudes by 9% on average (Fig. 2*D*). The addition of 100 μM NIF caused another small decline in fluorescence amplitudes, to an average 17% less than the original values, along with a concurrent increase of 30–100% in the baseline fluorescence.

Signal generation and propagation

By relying on the 1-D linear structure, it is possible to follow the firing sequence and identify the causality underlying the firing pattern. A fluorescent signal excited in a localized region with glutamate could be monitored as it progressed. The ability to measure linear propagation velocities enables a numerical comparison with theoretical models of signal propagation in neurons (see following text).

The cultures were locally stimulated by loading the pipette with either 20 or 200 μM of glutamate. The stimulation was in an all-or-none fashion with a minimal threshold and did not scale with the duration of exposure to glutamate. Usually around 100 ms was enough to evoke activity but the injection

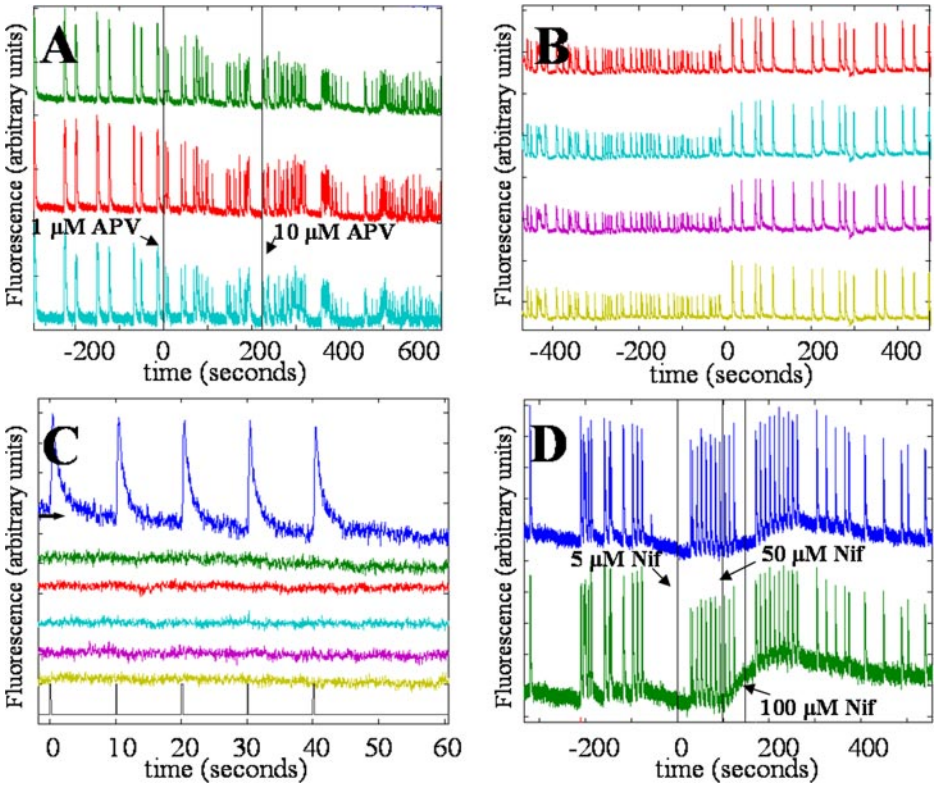

FIG. 2. Pharmacological treatment on patterned cultures. Each trace describes the average fluorescence in a different area of the culture. *A*: adding 1 μM of the *N*-methyl-D-aspartate (NMDA) channel antagonist 2-amino-5-phosphonovaleric acid (APV) globally at $t = 0$ (marked by first vertical line) causes an immediate decrease of around 30% in all areas of the culture. Raising the concentration of APV to 10 μM (second vertical line) eventually causes the amplitude to decrease to around 50% of the original values. *B*: bicuculline was added globally at $t = 0$, and caused a 2-fold increase in amplitudes in all areas of the culture. Increase was as high as 5-fold in other instances. Rate of bursts also dropped by a factor of about 4. *C*: 200 μM glutamate was locally applied to a specific area of the culture (whose fluorescence time course is depicted in the *topmost plot*, marked by an arrow), in the presence of 10 nM tetrodotoxin (TTX) in the whole sample. Spikes in bottom line signify points of stimulation. Whereas the area perfused by the pipette reacts to the stimulation, other areas (at distances from 0.4 to 4 mm from the pipette) show no reaction. (Compare with the case of no TTX in Fig. 3*B* below.) *D*: at $t = 0$ (marked by line), 5 μM of nifedipine was added to the culture. Different areas of the culture had different magnitudes of decrease in signal, from no effect to a 20% decrease, with a 9% decrease on average. Shown are 2 regions that exhibit an average decrease of 8 and 20%. Second and third vertical lines mark concentration increases to 50 μM and then to 100 μM. After this increase the amplitudes dropped to an average 17% less than the original values, and there was also a rise in baseline fluorescence.

time needed to excite such a response ranged from 20 ms to 1 s. We speculate that the measured time until the fast, large-amplitude phase appears is a combination of the efficiency of delivery of the drug and variation in the time until a large enough population of neurons, necessary to induce large-scale response, is activated. The efficiency of the delivery depends on local details of the area in the culture that is directly under the concentric pipette, such as the number of neurons (or synapses) that are actually exposed. The time that passes until a large-scale response is evoked may depend on the network connectivity of those neurons that are directly stimulated by the concentric pipette. Glutamate stimulation was subject to a refractory period of 3–10 s from the previous event, similar to electric stimulation (Maeda et al. 1995; Murphy et al. 1992).

Figure 3*A* demonstrates the geometry of the experimental system and the areas that were monitored on the video screen for changes in fluorescence intensity. The line was stimulated at a certain area and the initiation time of each event on each of the selected areas was then measured (Fig. 3, *B* and *C*). The results obtained by averaging these times (as measured from the time of stimulation) are shown in Fig. 3, *D–F*.

In Fig. 3, *D–F* the point of initiation is very clear. From this point the signal grows to include more neurons and advances, first at a slow velocity for a short distance, and then at a very fast one. Such a phenomenon was previously discussed by Osan and Ermentrout (2002). In Fig. 3*D* a slowing down of the signal propagation through the narrowing of the line at *area 5* is apparent, even though the initial slow velocity is obscured by large error bars. This is similar to the phenomena of slowing down at narrow passages seen in heart cultures (Rohr and Salzberg 1994) and when partial sectioning by laser is performed in neural cultures (Maeda et al. 1995). An explanation for the retardation of the spread of activity through a narrowing is offered below (see Fig. 4). To measure the velocity of the slow propagation, the same analysis was repeated with smaller areas close to the initiation point (see Fig. 5).

From the raw data (Fig. 3, *B* and *C*), one can detect that the fluorescent signal itself divides into two stages. At first, a slow rise of intensity appears around the stimulated area, and gradually the signal spreads to neighboring areas. Then, the center of activity exhibits a sharp jump in amplitude of the activity, which propagates almost simultaneously all along the line.

The second stage is thus characterized by fast propagation and higher amplitudes (Fig. 3*G*). The times at which the fluorescence signal reaches the greatest enhancement (highest derivative) constitute a typical sign of the fast propagation. There are cases in which there is no transition to a high-amplitude wave; in this case the slow front decays within $<$500

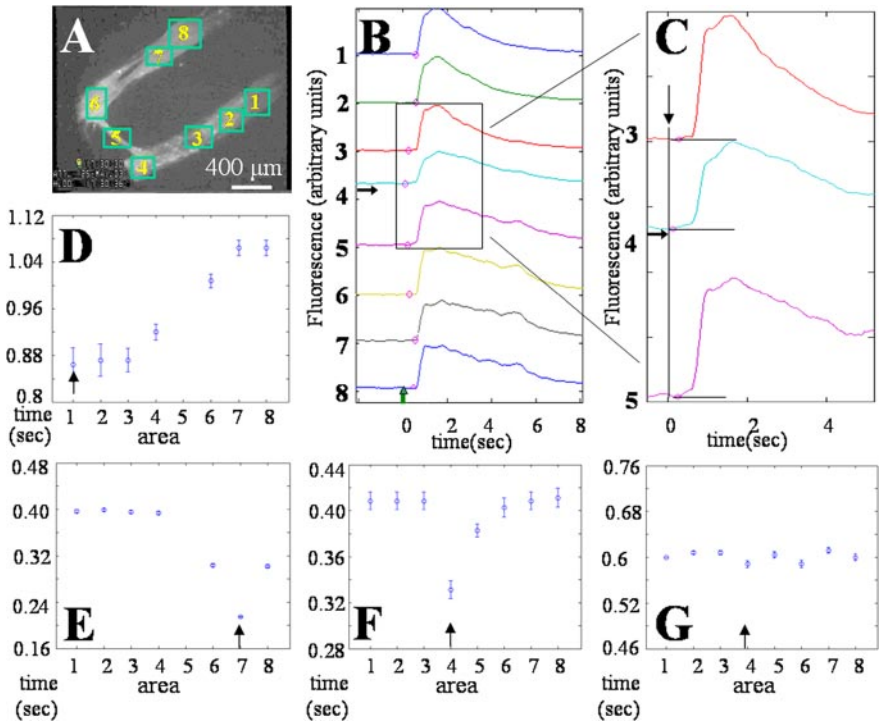

FIG. 3. Response of a linear network to glutamate stimulation. *A*: geometry of the network is depicted in this fluorescence image of Fluo-4–loaded cells. Eight regions of interest were selected in the culture and their mean fluorescence intensity was measured every 20 ms. *B*: a typical event. Time series of the fluorescence level (in arbitrary units) in the different areas after a single stimulation at *area 4* (arrow). Event initiation times are automatically found and marked on each plot. At *bottom* the stimulation signal is depicted as an arrow. *C*: enlargement of the areas near the stimulating pipette in *B*. Two stages are evident: a slow rise beginning at the onset of a (200-ms) glutamate application at $t = 0$, which develops into a sharp rise in fluorescence. *D–F*: average initiation time in the different regions of interest, relative to the beginning of a (200-ms) glutamate pulse applied near *areas 1*, *7*, and *4*, respectively (see arrows). In *D* retardation through *area 5* is seen, but large error bars hide the initial slow velocity. *G*: stimulating at *area 4*, the time of largest enhancement (highest derivative), indicative of the fast signal propagation, was measured for the same areas as before. Here we can discern no clear evidence of order because of the limitations of the video, and the different areas react simultaneously within video resolution.

μm of the initiation point. This instability of the slow propagating activity was predicted by Bressloff (2000).

The appearance of an initial slowly advancing activity that leads to the fast propagating activity is also observed in spontaneously generated activity. Furthermore, the passage of spontaneous activity through a very narrow area shown in Fig. 4, *A* and *B*, also demonstrates how the advance of the signal is retarded (the geometry is demonstrated in Fig. 4*G*). In this instance active neurons in *area 1* were insufficient to excite fast propagating activity through a constriction to *area 2*. Instead, a slow and low-amplitude activity, characteristic of the signal's initiation period, is transmitted. This may in turn excite high-amplitude activity in the area beyond the constriction, which propagates onward (Fig. 4*B*). Again, in the cases in which there was no transition to high-amplitude activity (Fig. 4*A*), the slow activity beyond the constriction decayed within <500 μm. The time until the fast propagation is similar to the time needed for the pipette to excite the fast propagating activity. Using the concentric double pipette it was possible to reversibly induce a similar attenuation and retardation effect on the activity of neurons growing on a line that does not have any special architecture. A line with constant thickness (170 μm, as shown in Fig. 4*H*) passes the signals with no retardation (Fig. 4*C*). However, once TTX was locally applied at the midpoint between two areas on the line it caused either propagation failure (Fig. 4*D*) or a delay in propagation (Fig. 4*E*). A fast recovery of the propagation was achieved once TTX application was stopped (Fig. 4*F*).

The slow and fast propagation velocities are demonstrated in Fig. 5. The geometry and chosen areas are once again shown for the sake of clarity (Fig. 5*A*). To follow the slow propagation a large number of areas near the initiation site (*area 1*) were chosen. In Fig. 5*B* the average time that passed from initiation of the signal in *area 1* until initiation of the signal in each area is plotted as a function of the distance of that area from *area 1*. At large distances fast propagation takes over and the times for initiation are almost uniform because of the low resolution obtained from following fluorescence signals with video. However, at small distances the slow propagation is quite evident.

The *inset* to Fig. 5*B* shows distance as a function of time, from which a constant average velocity (derivative) of about 1.5 mm/s can be obtained for this specific culture. After averaging ($n = 50$ events on three lines) the measured velocity is 2 ± 0.4 mm/s up to a distance of about 300 μm. Such a slow initial wave speed may be the result of a recruitment time or buildup period of population bursts, lasting 100–300 ms, and was reported experimentally in Menendez de la Prida and Sanchez-Andres (2000) and Sanabria et al. (2001). The slow velocity was also observed in the presence of bicuculline and APV, when most of the transmission occurs by AMPA synapses (see *inset*). Under these conditions, the average value of the slow velocity is 14.7 mm/s ($n = 3$ cultures). For both cases the slow propagation is well fit by a linear behavior, indicating constant velocity. This supports the use of a wavelike model (see following text) to explain the slow velocity.

To measure the fast propagation the limitation in time resolution caused by video imaging was to be overcome. To this end longer (17 mm) lines had to be used to enable a time span over which the fast front could be measured. An important property of 1-D networks is the ability to wind a long line on itself. This allows fitting long lines onto small cover glasses or viewing distant areas of the culture in a single microscopic field of view. The two ends and the central part of a 17-mm line were simultaneously visualized by patterning it in the shape of an elongated and thin "C" (see Fig. 6). The measured fast velocities depend on which synapses were blocked and range between 40 and 110 mm/s.

The fast velocities were measured along the lines in three states, and each measurement on a line included between 20 and 70 events:

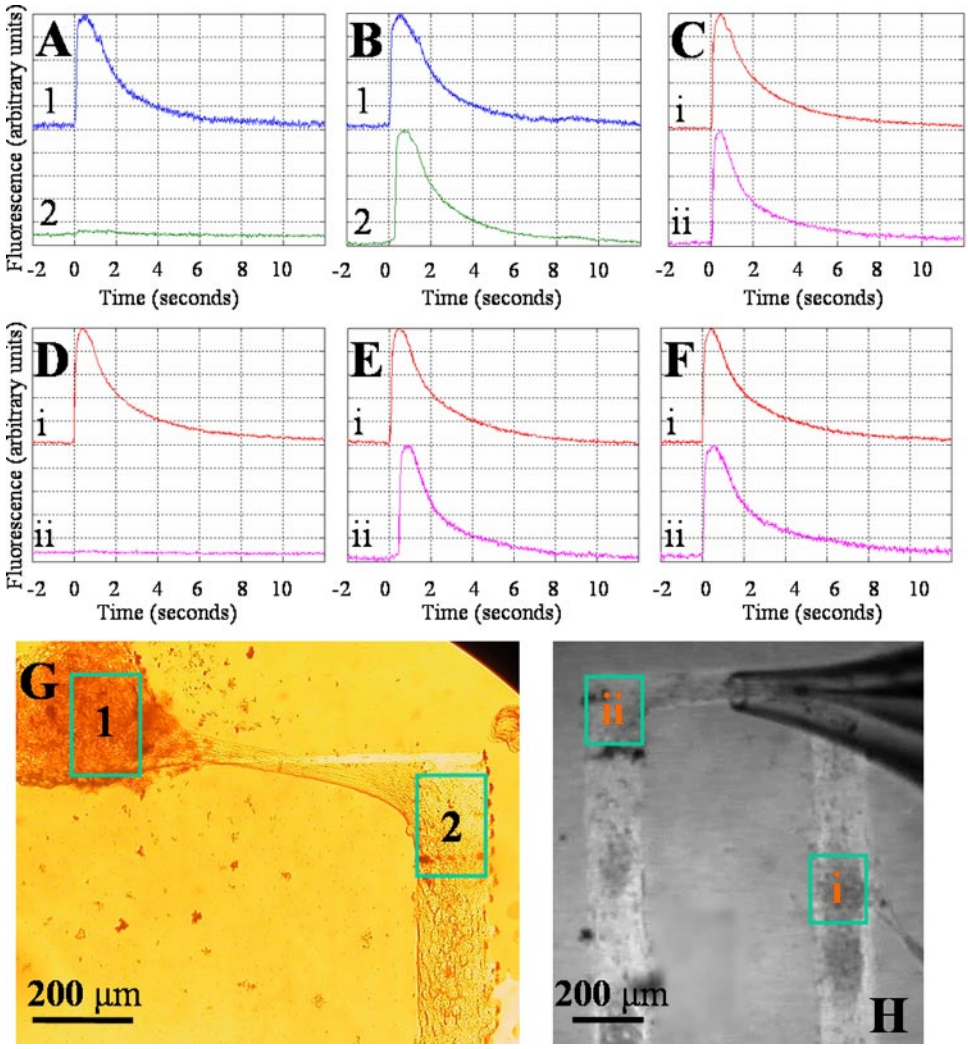

FIG. 4. Signal transmission through obstructions in the line. *A*: a single spontaneous event in 2 areas connected by a very thin line (about 400 μm long) that allows axons to pass through but cannot support soma adhesion (as shown in *G*). An event at *time 0* in *area 1* induces a slight response in *area 2*. This does not develop into a large-amplitude response at *area 2*. Around 50% of the events were of this nature. *B*: same 2 areas. An event is initiated at *time 0* in *area 1*, which excites *area 2*, where a new recruitment period seems to take place. A full-fledged event is visible in *area 2* only about 80 ms later. Around 50% of the events were of this nature. *C–F*: a similar phenomenon can be reversibly induced in a 4-mm-long, 170-μm-thick line by local pharmacology. A double pipette loaded with 1 μM TTX is placed between 2 areas (*i* and *ii*) as shown in *H*. *C*: before TTX application the signal passes between the 2 areas with no significant delay. *D*: during application of TTX a spontaneous event occurs at *area i*, which does not cross the "TTX barrier" to induce a full event on *area ii*. Around 70% of the events were of this nature. *E*: about 30% of the signals did cross the TTX barrier and caused a delayed event on the other side, very similar in structure to that shown in *B*. *F*: after TTX application is ceased the effect is reversed (usually within 0–2 events) and the signal again passes with no delay. *G*: a thin connection that does not support cell adhesion but can support axons. Data of *A* and *B* were taken from *areas 1* and *2* on a similar culture grown on an identical pattern. *H*: *areas i* and *ii*, whose fluorescence time plots are given in *C–F*, are connected by a line of constant thickness. Areas are partially disconnected by local application of TTX using concentric pipettes at the location shown.

1) When no drugs are added to the bath and AMPA, NMDA, and GABA synapses are active the average propagation velocity was 55 ± 4.5 mm/s (averaged over seven lines).

2) In the presence of 40 μM bicuculline, which blocks inhibition, the average velocity went up to 97 ± 10 mm/s (averaged over six lines).

3) In the presence of 40 μM bicuculline and 10 μM APV, leaving AMPA as the dominant active synapse, the measured velocity was 72 ± 3 mm/s (averaged over five lines). This is the velocity most relevant to the model below.

These values for the fast velocity are close to those measured in 2-D cultures and slices. Maeda et al. (1995) obtained 50 mm/s on 2-D cultures, whereas Golomb and Amitai (1997) measured 130–190 mm/s in a slice, Chervin et al. (1988) measured 60–90 mm/s, and Wu et al. (1999) measured 30 mm/s in similar systems. A pair of fast and slow velocities was also reported in thalamocortical slice (Metherate and Cruikshank 1999) with a value for slow propagation on the order of 20 and 1,250 mm/s for the fast velocity. However, in that case the fast wave is attributed to axonal transmission and precedes the slow synaptic transmission one, in contrast to the two synaptic transmission velocities measured here.

To control the synaptic strength we added varying amounts of the AMPA antagonist CNQX. Velocities were measured at partially effective doses of CNQX to partially block AMPA currents, along with 40 μM bicuculline and 10 μM APV, blocking the GABA and NMDA synapses. Average propagation velocities ($n = 7$ cultures) are given in Fig. 7. Because the propagation velocity without CNQX varied (depending on preparation and temperature), we normalized all samples by the CNQX concentration at which 75 mm/s were obtained. Sufficiently high concentrations of CNQX result in complete blocking and a failure of the population bursts to propagate (Golomb and Amitai 1997; Osan and Ermentrout 2002). Complete blocking did not always occur at the same concentration of CNQX, which ranged from 400 to 1,400 nM. The slowest speed measured before complete blocking (averaged over $n = 5$ samples) is 39 ± 5 mm/s.

Comparison with predicted velocities

The measured velocities can be compared with the theoretical velocities predicted by the full solution of a simple integrate-and-fire model (Osan and Ermentrout 2002; Osan et al. 2004). Their solution to the integrate and fire equation is

$$V_T = g_{syn} S(c)$$

where V_T is the voltage threshold for firing, g_{syn} is the synaptic strength and $S(c)$ (after inserting units) is the calculated function of the velocity c

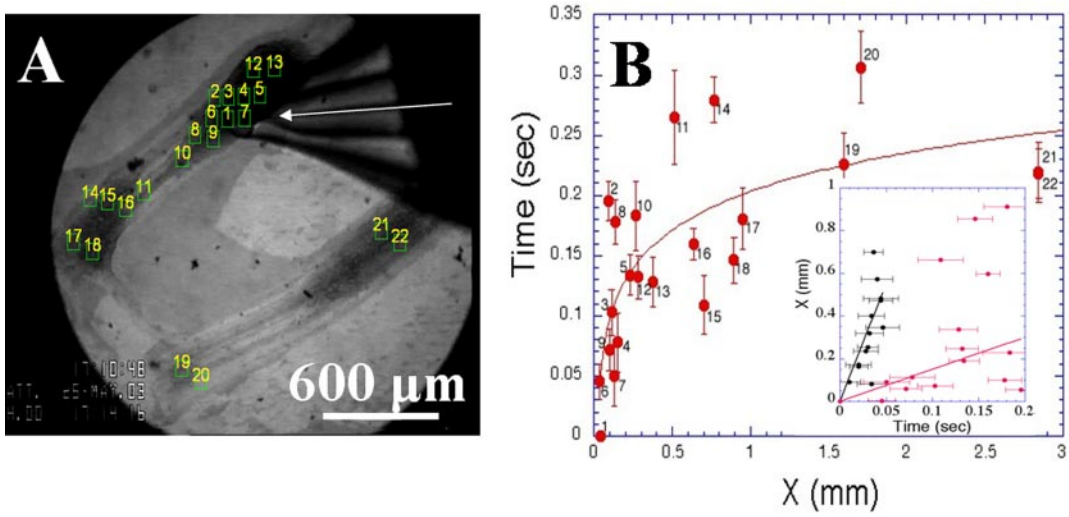

FIG. 5. Timing of fluorescence in different areas at varying distances from the stimulating coaxial pipettes. *A*: geometry and numbered areas of the culture on which the results shown in *B* were measured. Glutamate stimulation was performed near *area 1*. Response to each stimulation was measured in all areas. Stimulating pipette is visible on the *right top* (arrow). Pipette is above the sample and does not disturb the fluorescence measurements that are made from below. *B*: mean initiation time (relative to the time of stimulation) was measured for each area and plotted against the distance of that area from the stimulation site. Numbers correspond to those shown in *A*. *Inset*: distance vs. time for 2 experiments. Red dots are the data shown in the main graph and black dots are from an experiment in which only α-amino-3-hydroxy-5-methyl-4-isoxazolepropionic acid (AMPA) synapses were active. Lines are intended as a guide to the eye, indicating 1.5 mm/s for the red dots and 11 mm/s for the black dots. These lines are a good estimate only close to the site of initiation, where the signal has not yet evolved into the faster phase.

$$S(c) = \frac{a_1 a_2}{a_2 - a_1} \frac{\sqrt{\pi}}{\sqrt{2}} f\rho\tau w \left\{ e^{\left(\frac{wa_1}{c}\right)^2} \left[1 - \mathrm{erf}\left(\frac{wa_1}{c}\right) \right] - e^{\left(\frac{wa_2}{c}\right)^2} \left[1 - \mathrm{erf}\left(\frac{wa_2}{c}\right) \right] \right\}$$

Here erf is the error function; a_1 is the inverse of the membrane time constant at 28°C [$a_1 = 1/30\ \mathrm{ms}^{-1}$ (Borg-Graham 1998)]; and a_2 is the inverse of the synaptic (AMPA) time constant at this temperature, which is taken as $a_2 = 1/4\ \mathrm{ms}^{-1}$ (Borg-Graham 1998). The synaptic response function $A(t)$ given by Osan and Ermentrout (2002) is normalized and given dimensions by $\tau = 7.6$ ms

$$A(t) = g_{syn}\tau \frac{a_1 a_2}{a_2 - a_1} (e^{-a_1 t} - e^{-a_2 t})$$

This choice of τ sets the contribution from each presynaptic neuron to the postsynaptic potential to be g_{syn} in units of mV. ρ is the neuronal density that was measured to be $\rho = 0.31\ \mu\mathrm{m}^{-1}$ for the 170-μm-wide line, whereas $f = 0.8$ is the fraction of excitatory neurons in hippocampal cultures. The model assumes a Gaussian connectivity distribution with SD w, which is a very good description of the experimental distribution as well. The cumulative probability histogram of axon length obtained from Fig. 1*D* was used as a description of network connections. In this way an axon of length l contributes to all bins of length $\leq l$. This reflects the fact that axons may have boutons all along their length and not just at their furthest endings. This histogram is well estimated by a Gaussian distribution with SD $w = 288$ μm. Multiplying $S(c)$ by the number $\rho(\pi/2)^{1/2}w$ is a modification of the original model that translates the dimensionless notion of "connections per neuron" into numbers that derive from the physical parameters of the experimental system. The neurons' dendritic arbor is on the scale of the line width; therefore the wandering axon of a

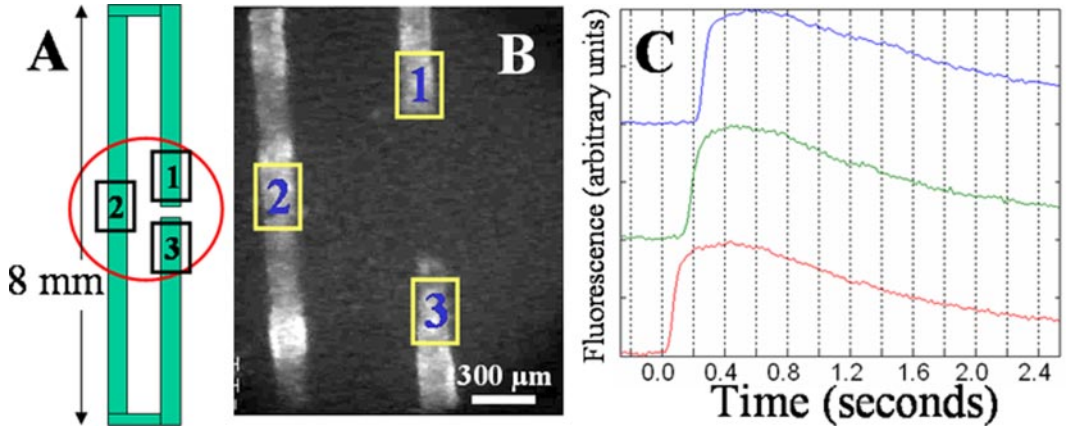

FIG. 6. Measuring fast velocities on 17-mm-long lines. *A*: schematic plot of a long line that was used. Microscope field of view is marked by a red circle and allows simultaneous visualization of *areas 1–3*. *B*: same 3 areas as viewed in fluorescent lighting. *C*: an event was initiated in *area 3* and traveled to *area 2* and then to *area 1*. Activity in the presence of 40 μM bicuculline. Relatively long distances between the 3 marked areas allow an accurate translation between signal onset differences in the 3 areas and the average signal velocity. In this instance the time delays are on the order of 100 ms, indicating a velocity of about 85 mm/s.

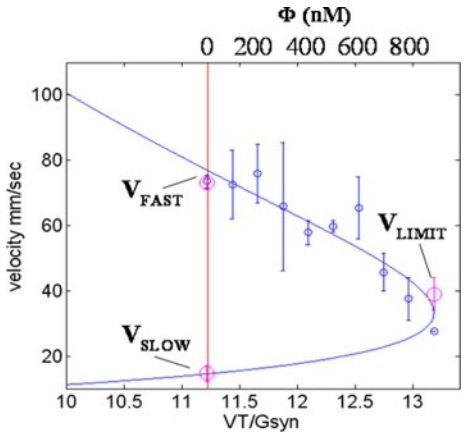

FIG. 7. Theoretical plot of velocities as a function of the ratio between the firing threshold and effective coupling (adapted from Osan and Ermentrout 2002). Two measured velocities of 15 and 72 mm/s (large circles colored magenta) correspond to a ratio V_T/g_{syn} of 11.2. Third large magenta circle (V_{LIMIT}) marks the average minimal velocity on addition of 6-cyano-7-nitroquinoxaline-2,3-dione (CNQX), before complete blockage, and is drawn at the turning point of the graph. Blue points are the measured velocities for different normalized CNQX concentrations, $\phi = 0$ to 900 nM where $\phi = 0$ is taken as the CNQX concentration for which the velocity was nearest 75 mm/s. Because of the low working concentrations of CNQX the first-order relation between ϕ and V_T/g_{syn} was used.

neuron may synapse onto any neuron within its reach (projected length from the soma).

The curve $S(c)$ is shown in Fig. 7. Given the fast velocity with AMPA alone of 75 mm/s, one can solve to get a second (slow) velocity of 15 mm/s (very close to the measured value of 14.7 ± 2.4 mm/s with AMPA alone). The model thus gives good predictions of both velocities, with the caveat that the moderate slope of the bottom branch in Fig. 7 may lead to substantial errors, mainly to an unreliable prediction for the synapse strength corresponding to the slow velocity. We also obtain in this step the value of $g_{syn} = V_T/11.2$, which implies that for synchronously firing presynaptic cells an integration from about 11 EPSPs is sufficient to induce a spike in a postsynaptic neuron.

On addition of varying concentrations of CNQX the measured velocities decreased until finally propagation failed. This is predicted by the theoretical model to occur at the turning point of the graph, where the velocity is 33.3 mm/s and $V_T/g_{syn} = 13.2$ (Fig. 7). For comparison, the slowest velocity that could be measured experimentally before complete blocking was 39 ± 5 mm/s, and is plotted using the same theoretical value of $V_T/g_{syn} = 13.2$.

DISCUSSION

The major characteristic of the patterned culture is the directionality of the axons. Although their length is not always much longer than the width, still the axons recognize the direction of the pattern, and most will grow parallel to it (projected distance is almost equal to the real distance). This is more in step with the directional behavior of neurons on a slice than in a 2-D culture, where the axons are less "well behaved" and wander about in a seemingly random walk. Even though the neurons do not arrange in single file (i.e., each neuron does not connect only to its two nearest neighbor), there are only five to ten of them in the width of the patterned line. Because of the distribution of axon lengths, it can be concluded that the probability of two neurons to connect diminishes with their distance. This locality condition is necessary for the theoretical model that was used.

The activity of the culture was verified by pharmacological means and was shown to be comparable to that of a normal 2-D culture. It is similar to activity observed in hippocampal slices (Menendez de la Prida and Sanchez-Andres 2000; Stoop and Pralong 2000), 2-D (Maeda et al. 1995; Muller and Swandulla 1995; Murphy et al. 1992), and 1-D cortical cultures (Segev et al. 2002). These bursts are argued to be of relevance to in vivo activity by Beggs and Plenz (2003, 2004), Engel et al. (1992), Gutnick et al. (1982), Lisman (1997), Meister et al. (1991), Shatz (1990), and Yuste et al. (1992). These pharmacological tests also prove that the measured fluorescent signals are indeed associated with synaptically mediated spiking activity. The propagating waves correspond to large-scale population bursts that travel along the line as neurons excite their neighbors.

The one-dimensionality gives a unique opportunity to evaluate causal progressive advance of population bursts along the line because the activity does not skip over an area along the line [as discussed by Buonomano (2003) this is somewhat different from the situation in slices]. This is related to the observation that the axons are far from extending the full length of the line, and activity has to be relayed by exciting neurons in the path of propagation. The fact that activity propagates as long as 8 cm from its initiation point shows that signals may pass as many as 240 times the mean axon length without decaying.

Although the 50-Hz video rate poses a 20-ms limit to the time resolution, in fact it was possible to obtain very good estimates of the propagation velocity of the activity front. The slow initiation velocity, on the order of millimeters per second, was easily observed at this time resolution, whereas for the fast velocities, a longer line (17 mm long) was used where the time between excitation of the different areas was long enough to resolve. As a result, causal propagation and the fast velocity could be measured. Although the slow propagation mode is well described by a linear fit (Fig. 5*B*), which suggests a wavelike propagation, it may also be fit otherwise. Furthermore, the model's prediction is somewhat weakened by the moderate slope of the slow velocity, along with relatively large error bars on the experimental data. Thus although our measurements support the model of Osan end Ermentrout (2002) we have not completely disqualified other mechanisms that may govern the initial slow phase, such as reaction diffusion processes.

Within the context of the theoretical model with synaptic transmission we can estimate the spread of incoming EPSPs over which a neuron integrates. This time interval is determined by the span of the axons and by the propagation velocity, both parameters of the model that are experimentally determined. This time window opens when the first EPSP reaches the neuron and closes when the neuron itself fires. Thus EPSPs are all concentrated within a window whose duration is the time lag between pre- and postsynaptic firing times, or the time it takes the population wave to travel the average distance between neuronal connections. For the slow velocity this leads to a spread of >30 ms. Because the membrane decay constant is on the order of 1/30 ms^{-1} this wave

must consist of asynchronous activity. In contrast, for the leading edge (at least) of the fast measured velocity this delay is <3 ms. Such a spread is much shorter than the characteristic decay time and can be related to synchronous activity. For the rest of the fast propagating wave this remains a conjecture that must be verified by electrophysiology, which we are currently undertaking. Such a transition from asynchronous to synchronous activity is discussed in theoretical models (Diesmann et al. 1999; Litvak et al. 2003).

One can now understand the origin of the two different propagating velocities in terms of synaptic transmission and synchronicity. During the initial period only a few neurons are activated. Because the number of excited neurons is small at first, the probability of postsynaptic neurons to receive enough simultaneous EPSPs and spike is also small, and thus the activity initially has small amplitude. Because their neighboring neurons are the ones that have a higher number of connections to them, their probability of firing is higher, and the initial activity is confined to the close vicinity of the stimulation. This process causes the initial propagation velocity of the activity to be slow. Once enough neurons (specifically, beyond a measured threshold of about 11 inputs per neuron) are firing, a synchronized bursting event (Abeles 1991) can be excited. We associate the high-amplitude, fast-velocity activity with such a synchronization of the neuronal firing activity.

This can also explain the retardation of a propagating wave beyond a constriction in the line. The neurons beyond the constriction receive a small number of synaptic inputs, causing only a fraction of them to react and leading to a delay and possible loss of synchronicity. This is similar to the situation in which an event is first initiated, and thus the same behavior of low- and then high-amplitude activity is detectable in this case.

It may now be inquired what are the rate limiting factors for the velocity of propagation of such population bursts. Estimates of action potential velocities in unmyelinated rat hippocampal axons (measured in slice preparations) are around 300 mm/s (Berg-Johnsen and Langmoen 1992; Candy and Szatkowski 2000; Kandel et al. 1991), whereas the fast velocity measured here is at most 110 mm/s. Although there is some temperature dependency, the effect of cooling down from 37 to 28°C (the temperature used in our experiments) was measured to slow conduction velocities in unmyelinated axons by about 100 mm/s (Berg-Johnsen and Langmoen 1992; Cottrell 1984), to a velocity still higher than the one we measured. Thus it is in fact likely that the synaptic transmission between neurons is the limiting factor for this velocity. In any case, the existence of two velocities, one of which is very slow, indicates that synaptic transmission is of great relevance. The slow velocity can be linked to the period until a large enough population, which is needed to initiate the fast velocity signal, becomes synchronously active. The model of Osan and Ermentrout (2002) deals precisely with this kind of situation, in which synaptic transmission is modeled whereas axonal propagation is ignored because it is assumed to be faster. It is therefore reasonable to use the model to describe this system and indeed the comparison is excellent to a high quantitative degree.

In conclusion, the one dimensionality of the cultures has allowed the causal progress of a signal from point to point to be monitored. The geometry of the network and its connectivity have been characterized, indicating that the density of neurons, and therefore the width of the line, constituted a good parameter for quantifying the connectivity. This has enabled the extraction of reliable and reproducible velocities for signal propagation in the network. Two regimes were found, one of which is a recruitment time during which neighboring neurons are excited. This initial stage ends with a transition to a large-amplitude "avalanche" in which the signal gains significantly both in amplitude and in speed, and this is the main mode of information transfer along the line. The same physical structure of the network supports two velocities, even if only one type of synapse is active. Such spontaneous transitions into a "synfire" mode were shown to have important implications on the ways that information may be coded in networks with a layered architecture (Abeles 1991; Diesmann et al. 1999; Litvak et al. 2003).

The unidimensionality also facilitates a direct comparison with the theory of Osan and Ermentrout (2002). The excellent quantitative agreement implies that the model captures the essential ingredients of synaptic transmission and also gives a numerical value for the synaptic connectivity of the network. It then helps to link synchronicity to high propagation velocities and asynchronous activity to low velocities.

Local application of glutamate with high spatial and temporal precision using concentric pipettes allows signals to be stimulated at different points, and their propagation to be followed through a variety of conditions and constrictions. We showed that the need to activate enough neurons beyond a constriction and reignite the signal is the probable cause for the delay of the signal as it crosses a constriction.

ACKNOWLEDGMENTS

We thank V. Greenberger, I. Fishbein, and R. Tal for biological aid and I. Ginzburg for discussions, advice, and for supplying us with the TAU-GFP construct. We also thank O. Bab and T. Shenhav for technical support.

GRANTS

The work was supported in part by the Israel Science Foundation Grant 298/01 and by the Minerva Foundation, Munich.

REFERENCES

Abeles M. *Corticonics: Neural Circuits of the Celebral Cortex*. Cambridge, UK: Cambridge Univ. Press, 1991.

Alitalo K, Kurkinen M, Virtanen I, Mellstrom K, and Vaheri A. Deposition of basement membrane proteins in attachment and neurite formation of cultured murine C-1300 neuroblastoma cells. *J Cell Biochem* 18: 25–35, 1982.

Beggs JM and Plenz D. Neuronal avalanches in neocortical circuits. *J Neurosci* 23: 11167–11177, 2003.

Beggs JM and Plenz D. Neuronal avalanches are diverse and precise activity patterns that are stable for many hours in cortical slice cultures. *J Neurosci* 24: 5216–5229, 2004.

Berg-Johnsen J and Langmoen IA. Temperature sensitivity of thin unmyelinated fibers in rat hippocampal cortex. *Brain Res* 576: 319–321, 1992.

Borg-Graham LJ. Interpetations of data and mechanisms for hippocampal pyramidal cell models. In: *Celebral Cortex: Cortical Models*, edited by Ulinski PS, Jones EG, and Peters A. New York: Plenum Press, 1998, vol. 13, p. 19–138.

Bressloff PC. Traveling waves and pulses in a one-dimensional network of excitable integrate-and-fire neurons. *J Math Biol* 40: 169–198, 2000.

Buonomano DV. Timing of neural responses in cortical organotypic slices. *Proc Natl Acad Sci USA* 100: 4897–4902, 2003.

Candy SM and Szatkowski MS. Neuronal excitability and conduction velocity changes in hippocampal slices from streptozotocin-treated diabetic rats. *Brain Res* 863: 298–301, 2000.

Chang JC, Brewer GJ, and Wheeler BC. Modulation of neural network activity by patterning. *Biosens Bioelectron* 16: 527–533, 2001.

Chervin RD, Pierce PA, and Connors BW. Periodicity and directionality in the propagation of epileptiform discharges across neocortex. *J Neurophysiol* 60: 1695–1713, 1988.

Cottrell DF. Conduction velocity and axonal diameter of alimentary C fibres. *Q J Exp Physiol* 69: 355–364, 1984.

Diesmann M, Gewaltig MO, and Aertsen A. Stable propagation of synchronous spiking in cortical neural networks. *Nature* 402: 529–533, 1999.

Engel AK, Konig P, Kreiter AK, Schillen TB, and Singer W. Temporal coding in the visual cortex: new vistas on integration in the nervous system. *Trends Neurosci* 15: 218–226, 1992.

Feinerman O and Moses E. A picoliter "fountain-pen " using co-axial dual pipettes. *J Neurosci Methods* 127: 75–84, 2003.

Golomb D and Amitai Y. Propagating neuronal discharges in neocortical slices: computational and experimental study. *J Neurophysiol* 78: 1199–1211, 1997.

Gutnick MJ, Connors BW, and Prince DA. Mechanisms of neocortical epileptogenesis in vitro. *J Neurophysiol* 48: 1321–1335, 1982.

Kandel ER, Schwartz JH, and Jessel TM. *Principles of Neural Science.* East Norwalk, CT: Appleton & Lange, 1991.

Kistler WM. Stability properties of solitary waves and periodic wave trains in a two-dimensional network of spiking neurons. *Phys Rev E Stat Phys Plasmas Fluids Relat Interdiscip Topics* 62: 8834–8837, 2000.

Lisman JE. Bursts as a unit of neural information: making unreliable synapses reliable. *Trends Neurosci* 20: 38–43, 1997.

Litvak V, Sompolinsky H, Segev I, and Abeles M. On the transmission of rate code in long feedforward networks with excitatory–inhibitory balance. *J Neurosci* 23: 3006–3015, 2003.

Maeda E, Robinson HP, and Kawana A. The mechanisms of generation and propagation of synchronized bursting in developing networks of cortical neurons. *J Neurosci* 15: 6834–6845, 1995.

Meister M, Wong RO, Baylor DA, and Shatz CJ. Synchronous bursts of action potentials in ganglion cells of the developing mammalian retina. *Science* 252: 939–943, 1991.

Menendez de la Prida L, and Sanchez-Andres JV. Heterogeneous populations of cells mediate spontaneous synchronous bursting in the developing hippocampus through a frequency-dependent mechanism. *Neuroscience* 97: 227–241, 2000.

Metherate R and Cruikshank SJ. Thalamocortical inputs trigger a propagating envelope of gamma-band activity in auditory cortex in vitro. *Exp Brain Res* 126: 160–174, 1999.

Muller W and Swandulla D. Synaptic feedback excitation has hypothalamic neural networks generate quasi-rhythmic burst activity. *J Neurophysiol* 73: 855–861, 1995.

Murphy TH, Blatter LA, Wier WG, and Baraban JM. Spontaneous synchronous synaptic calcium transients in cultured cortical neurons. *J Neurosci* 12: 4834–4845, 1992.

Osan R, Curtu R, Rubin J, and Ermentrout B. Multiple-spike waves in a one-dimensional integrate-and-fire neural network. *J Math Biol* 48: 243–274, 2004.

Osan R and Ermentrout B. The evolution of synaptically generated waves ine one- and two- dimensional domains. *Physica D* 163: 217–235, 2002.

Papa M, Bundman MC, Greenberger V, and Segal M. Morphological analysis of dendritic spine development in primary cultures of hippocampal neurons. *J Neurosci* 15: 1–11, 1995.

Rohr S and Salzberg BM. Multiple site optical recording of transmembrane voltage (MSORTV) in patterned growth heart cell cultures: assessing electrical behavior, with microsecond resolution, on a cellular and subcellular scale. *Biophys J* 67: 1301–1315, 1994.

Sanabria ER, Su H, and Yaari Y. Initiation of network bursts by Ca^{2+}-dependent intrinsic bursting in the rat pilocarpine model of temporal lobe epilepsy. *J Physiol* 532: 205–216, 2001.

Segev R, Benveniste M, Hulata E, Cohen N, Palevski A, Kapon E, Shapira Y, and Ben-Jacob E. Long term behavior of lithographically prepared in vitro neuronal networks. *Phys Rev Lett* 88: 118102, 2002.

Shatz CJ. Impulse activity and the patterning of connections during CNS development. *Neuron* 5: 745–756, 1990.

Siegal RM and Read HL. Deterministic dynamics emerging from a cortical functional architecture. *Neuron Netw* 14: 697–713, 2001.

Stoop R and Pralong E. Functional connections and epileptic spread between hippocampus, entorhinal cortex and amygdala in a modified horizontal slice preparation of the rat brain. *Eur J Neurosci* 12: 3651–3663, 2000.

Wu JY, Guan L, and Tsau Y. Propagating activation during oscillations and evoked responses in neocortical slices. *J Neurosci* 19: 5005–5015, 1999.

Yuste R, Peinado A, and Katz LC. Neuronal domains in developing neocortex. *Science* 257: 665–669, 1992.